Article

Comparison Direct Synthesis of Hyaluronic Acid-Based Carbon Nanodots as Dual Active Targeting and Imaging of HeLa Cancer Cells

Yu-Yu Aung, Aswandi Wibrianto, Jefry S. Sianturi, Desita K. Ulfa, Satya. C. W. Sakti, Irzaman Irzaman, Brian Yuliarto, Jia-yaw Chang, Yaung Kwee, and Mochamad Z. Fahmi*

Read Online

ACCESS | Metrics & More | Article Recommendations | SI Supporting Information

ABSTRACT: The present study explores the potential of carbon nanodots (CDs) synthesized from hyaluronic acid using microwave-assisted and furnace-assisted methods as bioimaging agents for cancer cells. The investigation on the effect of microwave-assisted and furnace-assisted times (2 min and 2 h) on determining CD character is dominantly discussed. Various CDs, such as HA-P1 and HA-P2 were, respectively, synthesized through the furnace-assisted method at 270 °C for 2 min and 2 h, whereas HA-M1 and HA-M2 were synthesized with the microwave-assisted method for 2 min and 2 h, respectively. Overall, various CDs were produced with an average diameter, with the maximum absorption of HA-P1, HA-P2, HA-M1, and HA-M2 at 234, 238, 221, and 217 nm, respectively. The photoluminescence spectra of these CDs showed particular emissions at 320 nm and excitation wavelengths from 340 to 400 nm. Several characterizations such as X-ray photoelectron spectroscopy, Fourier-transform infrared spectroscopy, X-ray diffraction, and Raman spectroscopy reveal the CD properties such as amorphous structures, existence of D bands and G bands, and hydrophilic property supported with hydroxyl and carboxyl groups. The quantum yields of HA-M1, HA-M2, HA-P1, and HA-P2 were 12, 7, 9, and 23%, respectively. The cytotoxicity and in vitro activity were verified by a cell counting kit-8 assay and confocal laser scanning microscopy, which show a low toxicity with the percentage of living cells above 80%.
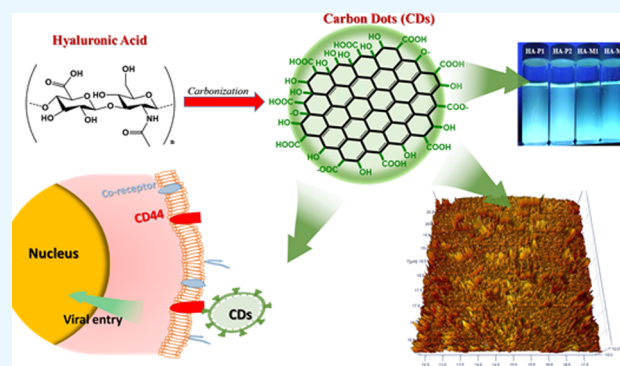
1. INTRODUCTION

Over the past 3 decades, cancer has been a common major problem and became one of the leading death causes in every country of the world.[1] In 2018, the International Agency for Research on Cancer predicted that 18.1 million new cancer cases and 9.6 million deaths will be reached in 5 years, the so-called 5-year prevalence, which is estimated to be 43.8 million.[2] Thus, several intensive attempts are being made for the development of therapies as worth as early diagnosis procedures. General cancer treatments that may be applied are surgery, chemotherapy, or radiotherapy. However, they are not effective due to the failure of early diagnosis, insufficient on-targeted drug delivery, systemic toxicity, and lack of real-time monitoring of therapeutic responses in cancer treatment.[3] Therefore, early detection of cancer is important to determine treatments that should be given to cancer patients.

Many efforts have been focused on the disease through innovative approaches in the biomedical field by recent advances in nanotechnology. The researchers are developing nanoparticles as smart tools for molecular imaging to determine the molecular-level detection of cancer. Nanoparticles are excellent optical probes that have fluorescent activity and passive targeting ability for light-scattering-based bioimaging and biomolecular detection.[4,5]

Various nanoparticles used for optical fluorescence imaging including mesoporous silica nanoparticles,[6] carbon nanotubes,[7] nanodiamonds,[8] semiconductor quantum dots (QDs),[9] gold nanoparticles,[10] and graphene[11] have been extensively studied for biomedical applications. Carbon-based QDs (also called carbon nanodots, CDs) have gained the attention of researchers due to their properties such as a small size of less than 10 nm, good hydrophilicity, biocompatibility, low cytotoxicity, fluorescence emission, chemical stability, easy synthesis, and other physicochemical properties.[12] Their optical properties and fluorescence emissions in the near-infrared spectral region make them a superior candidate for
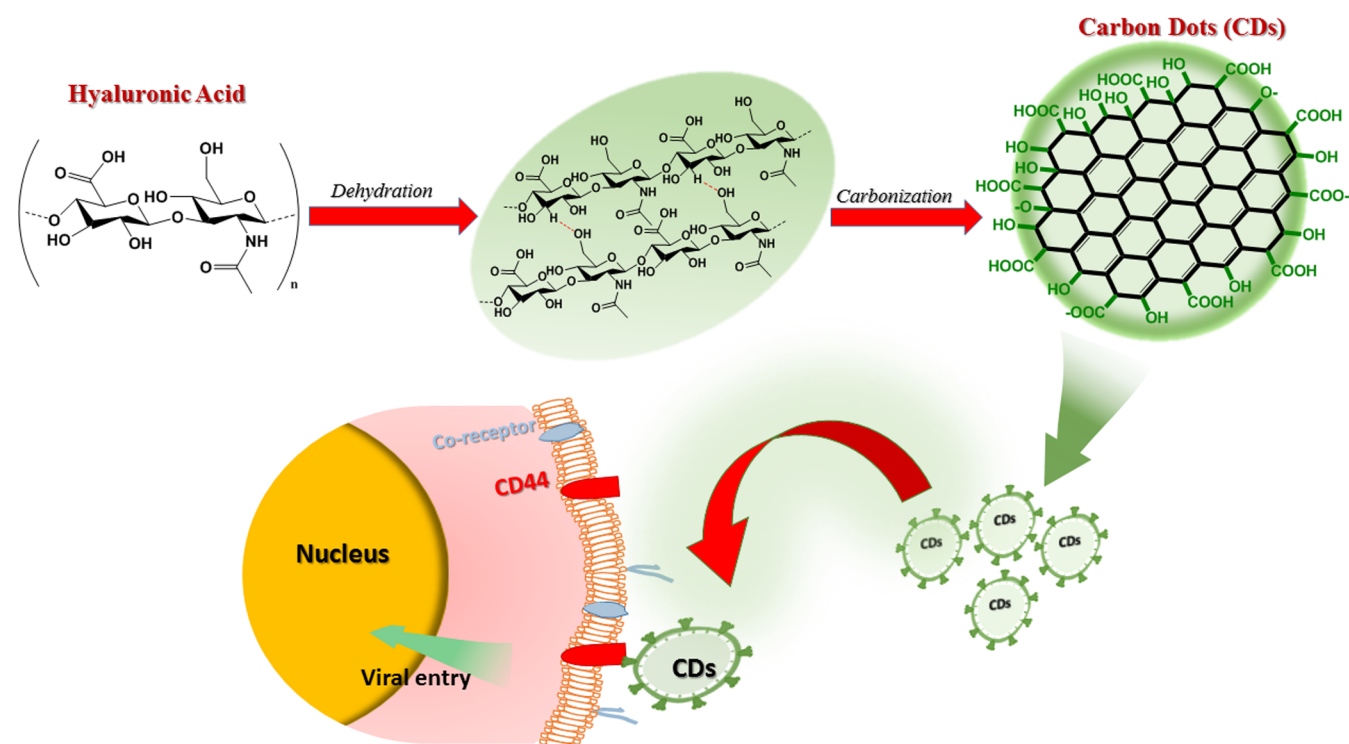
Scheme 1. Illustration of the Synthesis of HA CDs and Their Internalization Mechanism on HeLa Cancer Cells

biomedical applications, especially for bioimaging cancer detection, compared to other nanoparticles.[13]

CDs can be synthesized from several materials such as amino acids,[14] monosaccharides, polysaccharides,[15] citric acid,[16] and hyaluronic acid (HA).[17] Biomass polysaccharides are well-known as natural biopolymers, which are considered as water and energy storage, structural materials, and plants' suppliers. In recent advances, natural linear polysaccharide-based materials were used to synthesize many CDs due to their desirable properties such as non-toxicity, biodegradability, biocompatibility, non-immunogenicity, polymeric nature, and excellent hydrophilicity, which allow them to be widely used as prognostic molecules and in the treatment of various human and animal diseases.[18,19] Among various biomass-derived polysaccharides, HA is one of the carbon source precursors with multiple acid and hydroxyl groups set as a linear long-chain polymer, ubiquitous with a glycosaminoglycan group in the mammalian tissue and extracellular matrix.[20,21] In previous studies on cancer cells, HA is bound to a cluster-determinant 44 (CD44) receptor for targeting and activating over-expression in all cancer cells, which has high affinity as a desirable receptor compared to normal body cells. It indicated that HA can be a potential material for future applications in clinical cancer therapy and detection.[22]

CDs can be synthesized by two methods: top–down and bottom–up. However, top–down methods require external energy to break down relatively huge carbon molecules into smaller carbogenic parts based on physical approaches, such as arc-discharge,[23] arc-produced,[24] laser ablation,[25] electro-oxidation,[26] and electrochemical methods.[27] Meanwhile, bottom–up methods used carbon precursors to synthesize CDs based on chemical approaches. Bottom–up methods are simpler, and it is feasible to control experimental conditions with low-cost starting materials and experimental apparatus. Bottom–up methods include ultrasound-assisted,[27,28] pyrol-

ysis,[29] hydrothermal,[30] and microwave-assisted methods.[31] Among the above methods, the application of microwave- and furnace-assisted methods promoted simple, rapid, and efficient processes.[12] In terms of the application of HA as CD sources, recent studies have reported the application of the hydrothermal method on the synthesis of CDs using HA.[32−34] Even though the obtained CDs work successfully on theranostics of tumor cells, the hydrothermal method offering a multi-step, complicated synthesis process can also be attributed to those reports. These conditions motivate us to explore more applications of microwave- and furnace-assisted methods for CD synthesis. Moreover, the study on the application of HA in nanomaterial research predominantly just explores its function as a cancer-cell-targeting agent, and the synthesis of HA-based CDs has not been clearly explored yet. In scope of effectiveness, it has become a crucial aspect to create a simple and fast synthesis route on preparing CDs as excellent theranostic agents.

In the present research, CDs were synthesized using HA as a carbon source through, while also comparing, microwave- and furnace-assisted methods for their use as a HeLa marker. The as-prepared CDs were further characterized to determine the structure, fluorescence, and bioimaging application. The toxicity of CDs was measured using a cell counting kit-8 (CCK-8) assay, and the CD fluorescence imaging on HeLa cells was acquired by confocal laser scanning microscopy (CLSM). Other optical and structural characterizations on CDs were also determined, including X-ray diffraction (XRD), Fourier-transform infrared (FTIR) spectroscopy, Raman spectroscopy, X-ray photoelectron spectroscopy (XPS), and UV−vis spectroscopy.

2. RESULTS AND DISCUSSION

The comprehensive mechanism of CD formation involves dehydration and carbonization in the progress of microwave-

and furnace-assisted experiments using HA as shown in Scheme 1. We designed HA as carbon precursors, while sodium hydroxide was used to activate the formation of CDs through regular dehydration, followed by carbonization. The existence of NaOH encourages any electronegative site of HA to support removal of water through first dehydration and further carbonization to form graphene oxide-like structures on CDs. HA has a high affinity as desirable receptors for targeting and activating overexpression in cancer cells due to its ability to bond with CD44 receptors. The CD formation was proven by the emission of luminescence of CDs under UV light (Figure 1a). This phenomenon came surely from electron movement on the orbital state of CDs.
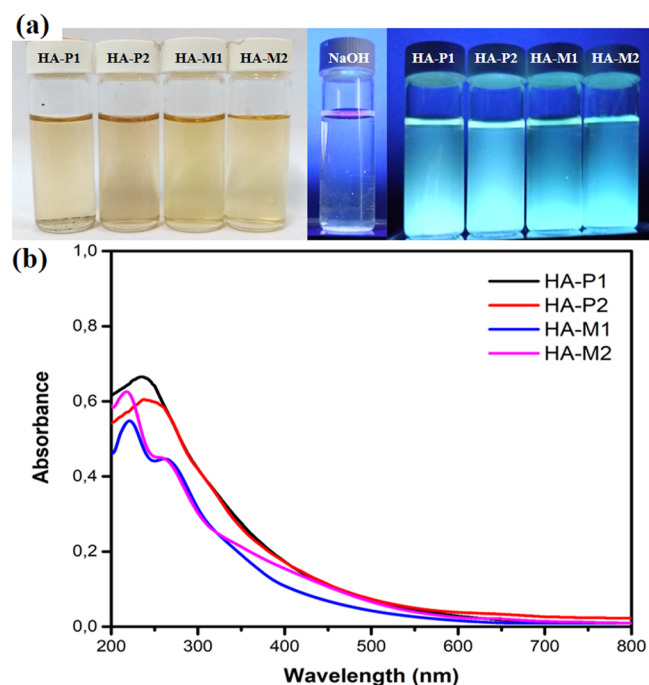

Figure 1. (a) Photograph of HA CDs taken under 320 nm UV light. (b) UV−vis spectra of furnace-assisted CDs, which are referred to as HA-P1 (black line) and HA-P2 (red line). UV−vis spectra of the microwave-assisted CDs, referred to as HA-M1 (blue line) and HA-M2 (purple line).

All CD emissions are mainly influenced by the sp^2 hybridization by the conjugation bond in the core of CDs and the functional and chromophore groups on the surface of CDs.[35,36] In order to investigate the qualitative analysis of the surface state and the conjugation bond of CDs, further analysis results are illustrated in Figure 1b. The UV−vis absorption spectra of CDs showed a broad absorption band in the range of 200−800 nm. The spectra for HA-M1 and HA-M2 both show two typical absorption maximum peaks at approximately 217 and 283 nm. Meanwhile, HA-P1 and HA-P2 exhibited absorption peak of the $\pi-\pi^*$ transition of the sp^2 carbon core or C═C bonds at 262 nm and that of the $n-\pi^*$ transition of C═O bonds at 284 nm.[37] It confirmed that CDs have a typical aromatic π system similar to the polycyclic aromatic hydrocarbon structure.[19] In general, CDs obtained a maximum absorption wavelength range of 260−320 nm.[38] The CDs are relatively more efficient at high absorption wavelengths. Their absorption characteristics are different from each other, which depend on surface passivation and functional groups of CDs.[39]

For further investigation on the optical properties of CDs, we assess photoluminescence (PL) spectra of pure HA (Figure 2a) utilizing furnace-assisted CDs (Figure 2b,c) and microwave-assisted CDs (Figure 2d,e). This analysis aims to acquire the emission wavelength, emission characteristics, and quantum yield (QY) value of compared CDs. For all samples, fluorescence occurred at around 410−445 nm by applying λ_{ex} = 320 nm, which also emitted a strong light-blue color.[33] The alteration of the excitation wavelength from 420 to 510 nm caused the PL peak of CDs to shift at a longer wavelength with a maximum intensity, which tends to form a red-shift emission (Figure 2f).[32] The transition of the lowest unoccupied molecular orbital to the highest occupied molecular orbital can be observed by the PL spectra. Among these CDs synthesized with varied methods, the maximum intensity emission of HA-P2was found at a wavelength of 502 nm. The optical properties of CDs have different excitation wavelengths, with different QY values. Using rhodamine 6G (R6G) as a reference, the QY has been calculated as 95%.[40] The QYs of HA-M1, HA-M2, HA-P1, and HA-P2 were obtained as 12, 7, 9, and 23%, respectively. It can be observed that the QY of HA-P2 was the highest compared to that of other CDs and the previous studies as mentioned in Table S1. The PL properties of CDs were used as parameters to study the PL mechanism of these CDs, which were important to reach the highest PL of CDs.[41]

FTIR analysis was next implemented to verify functional groups identified on the CDs. FTIR spectra of bare HA, HA-M1, HA-M2, HA-P1, and HA-P2 are shown in Figure 3. The characteristic absorption bands of O−H and N−H stretching vibrations show a peak at 3353 cm^{-1}. The absorption peak represents stretching vibrations of carboxylic (COO^-) groups at 2933 cm^{-1}. The peaks were related to the asymmetric and symmetric stretching vibrations of carboxyl acid groups on the CD surface at around 1645−1341 cm^{-1}. The carboxyl stretching vibration group was stronger than the others on the CD structure. The peaks can be observed because of the C−H stretching vibrations and bending of sp^2 to sp^3 of the C−H group at 1049 cm^{-1}. This peak was stronger on HA-M1 than that on others.[42] It was confirmed that the surface of CDs contains hydrophilic functional groups such as carboxyl and hydroxyl groups. Based on these, CDs have good water solubility.[19] All samples were investigated even further using XPS in order to acquire the composition of elements and percentages and detailed chemical bonding of the samples. As shown in Figure 4, the C 1s spectra of HA-P and HA-M reveal three similar types of carbon bonds, such as sp^3 carbon (284 eV), sp^2 carbon (~285 eV), and C−O (~287 eV). It indicates that CDs HA-M and HA-P have conjugated structures of C═C and C═O, carboxylic groups, and also hydroxyl groups.[43] The N 1s spectra showed two peaks such as C−NH (399.4 eV) and N−(C═O) peaks (~400 eV), which correspond to pyrrolic/pyridinic and graphic N, respectively. The O1s spectra of HA-P1 and HA-M1 showed two peaks such as C−O (~531 eV) and C═O (533 eV) peaks. This shows that CDs are highly soluble and stable in an aqueous solution because of their oxygen-rich structure.[44] The results are in accordance with the XPS analysis, which shows hydrophilic groups such as −OH, −NH$_2$, and COO− on the surface of as-synthesized CDs.[45]

XRD analysis (Figure S1, Supporting Information) showed a broad peak in the diffractogram range between 20 and 30° for HA-M1. In contrast, HA-M2, HA-P1, and HA-P2 showed low
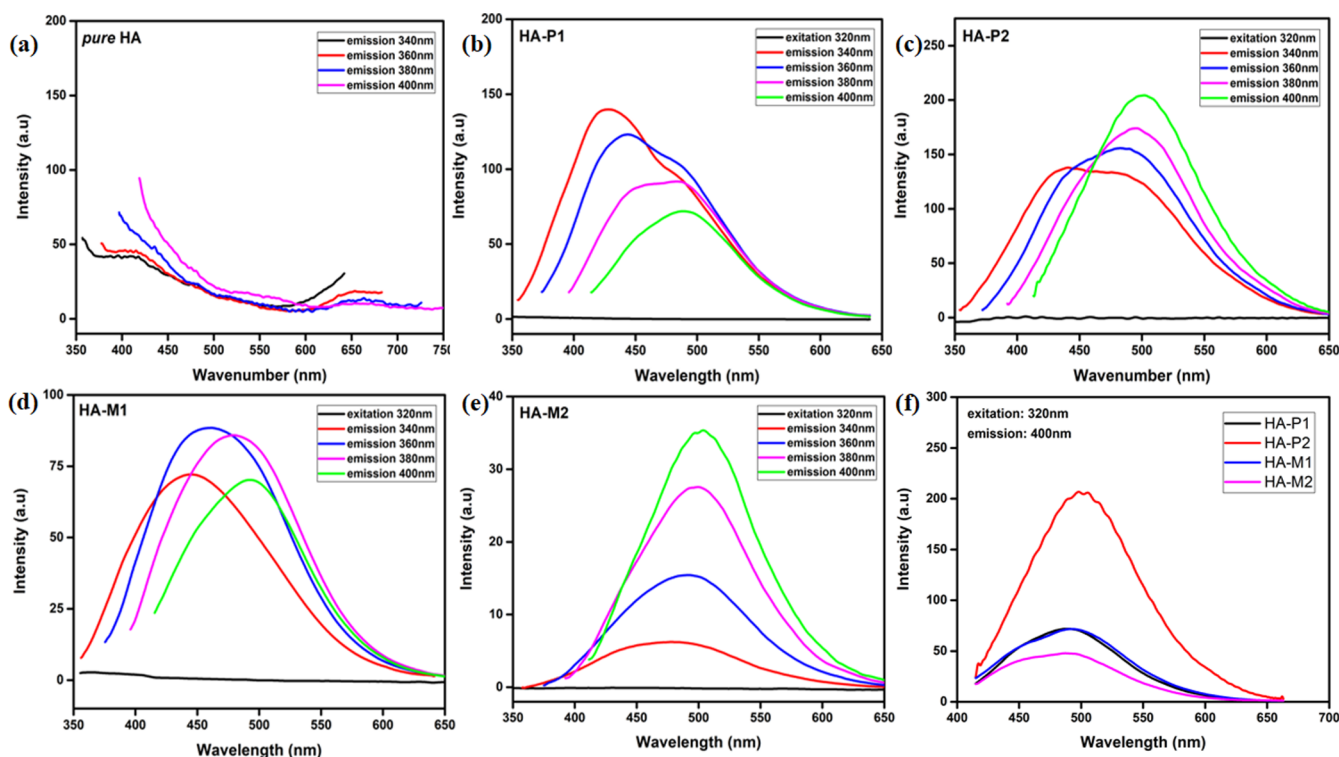
Figure 2. PL spectra of (a) pure CDs, (b) HA-P1, (c) HA-P2, (d) HA-M1, and (e) HA-M2 at varied values of λ_{ex}. (f) PL spectra of all CDs prepared by furnace-assisted and microwave-assisted methods at a λ_{ex} of 320 nm and a λ_{em} of 400 nm.
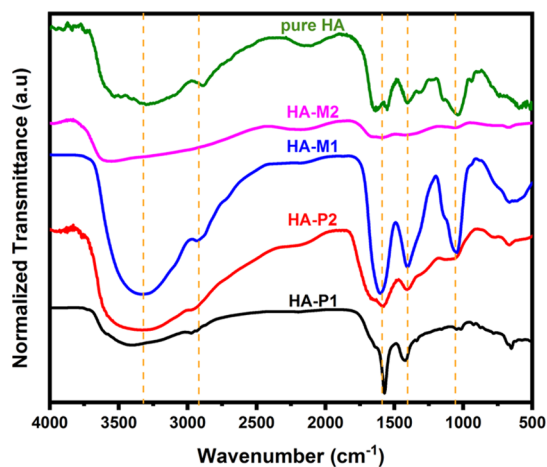

Figure 3. IR data of pure HA (green line), microwave-assisted CDs HA-M2 (purple line) and HA-M1 (blue line), and furnace-assisted CDs HA-P2 (red line) and HA-P1 (black line).

significant peaks to prove the crystallinity of CDs at these ranges. The peaks of CDs represent the amorphous carbon phase at a 2θ of about 22.7°.[46,47] Further analysis to determine the existence of graphene-like structures on HA CDs was performed using Raman spectroscopy (Figure 5a). Raman spectra showed the D bands of HA-M1, HA-M2, HA-P1, and HA-P2 at 1354, 1358, 1344, and 1371 cm^{-1}, respectively, which are attributed to the sp^3-hybridized formation of CDs.[48] In addition, the G bands of HA-M1, HA-M2, HA-P1, and HA-P2 at 1557, 1577, 1570, and 1570 cm^{-1}, respectively, refer to the presence of carbon with the sp^2 hybridization on CDs.[49] The appearance of the D band and G band on the surface of CDs leads to the formation of amorphous carbon.[50] Moreover,

the I_D/I_G ratios of all samples were measured in order to define the defect on CDs. The I_D/I_G ratios of HA-M1, HA-M2, HA-P1, and HA-P2 were obtained as 0.84, 0.70, 0.70, and 0.66, respectively. All CDs exhibited a decreasing number of D bands and an increasing number of G bands, demonstrating the disorderedness of sp^3 and sp^2 hybridizations that simply induced the formation of graphite structures or thinner graphene sheets.[51] The morphology of CDs was identified by atomic force microscopy (AFM) in order to discover the size distribution of CDs. The size distribution of HA-P2 is significantly calculated using ImageJ, where the mean diameter size is about 7 nm (Figure S2, Supporting Information). Furthermore, the three-dimensional (3D) topography of HA-P2 then displayed an average height of below 10 nm (Figure 5b), which means that HA-P2 is categorized in CDs.[52–54]

2.1. In Vitro Evaluation of CDs. Further observations of all CDs related to biomedical application were obtained by inspecting the capability of each CD for the staining of HeLa cell lines. The CCK-8 assay was conducted to determine the cytotoxicity of CDs. Figure 6 shows the cell viability of HA-M1, HA-M2, HA-P1, and HA-P2 under various concentrations. The result shows that HA-P2 has the maximum cell viability of 116.92% at 100 μg/mL. Meanwhile, HA-M2 shows minimum cytotoxicity with a cell viability of 91.28% at 5 μg/mL. The percentage of cell viability of samples was more than 80%, which indicates that the as-synthesized CDs had low toxicity.[55] Other studies (ISO 10993-5) have identified the cell viability in the range 80−120%, referring to the low toxicity on cells.[56,57] The cytotoxicity of the sample was compared with that of the untreated control with a cell viability of 100%. The cytotoxicity enhancement data have been intensively explored in determining the 50% cytotoxic concentration, or commonly called CC$_{50}$, of each of the varied CDs (Figure S3, Supporting Information). The fitting curve shows that for CDs HA-M1,
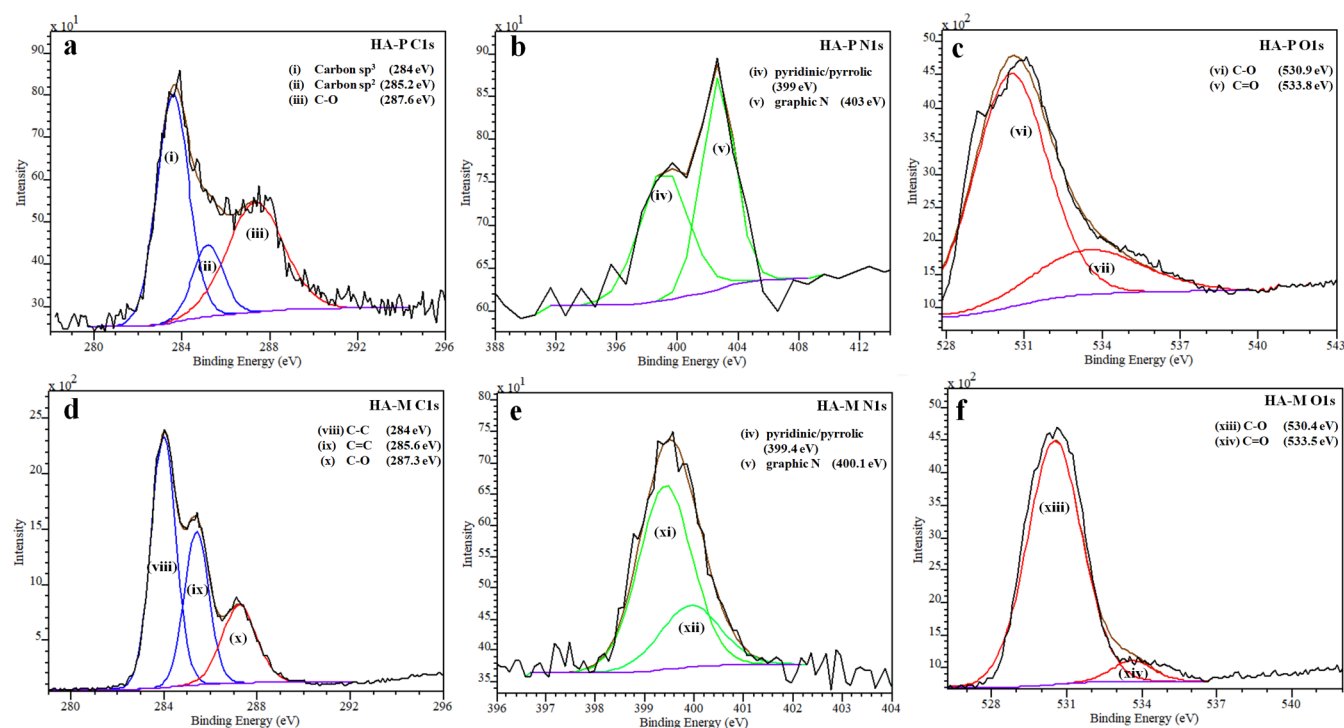
Figure 4. XPS spectra of microwave-assisted HA-M CDs: (a) C 1s, (b) N 1s, and (c) O 1s regions. XPS spectra of furnace-assisted HA-P CDs: (d) C 1s, (e) N 1s, and (f) O 1s regions.

HA-M2, HA-P1, and HA-P2, CC_{50} values are 1673, 54590, 2722, and 68587 μg/mL, respectively. Based on the result, the obtained CDs can be safely used in vitro and potentially applied for in vivo bioimaging studies even at high concentrations.[58]

CLSM evaluation was used to further investigate the capabilities of CDs as in vitro bioimaging agents. The HeLa cells incubated with HA-M1, HA-M2, HA-P1, and HA-P2 show excellent green fluorescence around an excitation wavelength of 488 nm (Figure 7), which demonstrates the outstanding cell selectivity of HA CDs as well as consistency in surface binding and absorption of CDs by cells.[59,60] Furthermore, the z-stacking mode in CLSM was also used in proving CDs in the cell cytoplasm. From the data in Figure S4, Supporting Information, it can be observed that the accumulation of CDs in cells constitutes an active targeting package as well as an endocytosis process to make them exist in the cell cytoplasm. Thus, the result exhibits an excellent fluorescence imaging of CDs, which has remarkably high photostability and biocompatibility.

3. CONCLUSIONS

Herein, we have synthesized CDs from HA using microwave-assisted and furnace-assisted methods. The resulting CDs have excellent fluorescence properties, high photostability, and biocompatibility that possess the potential for bioimaging and anti-cancer effects. The result shows that HA-P2 has a higher value of QY and cell viability than the other CDs. Luminescence and biocompatibility properties of CDs were confirmed by CLSM on HeLa cells and the CCK-8 assay, respectively. Thus, the one-pot-synthesized HA-based CDs that target CD44 HeLa cancer cells could be a promising way to improve cancer treatments.

4. EXPERIMENTAL SECTION

4.1. Materials. HA (97%), sodium hydroxide (NaOH, 99,8%), hydrogen chloride (HCl, 37%), ethanol (99.5%), Dulbecco's modified Eagle's medium (DMEM, high glucose), fetal bovine serum (FBS), and phosphate buffered saline (PBS) were purchased from Sigma-Aldrich Inc. CCK-8 was purchased from MedChenExpress Ltd. All chemicals were used directly without any specific purification.

4.2. Synthesis of CDs. In the present study, CD synthesis was similar to that described in the latest work with some variations,[36] namely, microwave-assisted and furnace-assisted methods. In the microwave-assisted method, 10 mg of HA was added to 300 μL of NaOH 0.1 N to form a dispersed solution. The mixture was stirred until a homogeneous and colorless gel was obtained. The mixture was then put into a microwave irradiation equipment (450 W) and continuously heated for 2 min (obtained CDs were marked HA-M1) and 2 h (obtained CDs were marked HA-M2). In the furnace-assisted method, about 10 mg of HA was heated at 270 °C for 2 min (obtained CDs were marked HA-P1) and 2 h (obtained CDs were marked HA-P2). Then, all CD products were purified by a dialysis process using a 1 kDa MWCO dialyzer (Orange Scientific) using deionized water for 24 h.

4.3. Cytotoxicity Evaluation of CDs. The breast cancer cells (HeLa cells) were seeded in a 96-well plate and cultured in DMEM (at a density of 3×10^4 cells/μL) containing 10% (v/v) FBS, 1% penicillin−streptomycin, and 1% 2 mM L-glutamine at 37 °C and 5% CO_2. After 24 h of incubation, the media were removed and washed three times with PBS. Then, carbon QDs were added to each well with varying concentrations, that is, 1, 2, 3, 5, 25, 100, and 400 μg/mL. Untreated cells were used as a negative control by adding solvents only. Thereafter, the formazan crystal was formed by adding 10 μL of the CCK-8 reagent to each well and
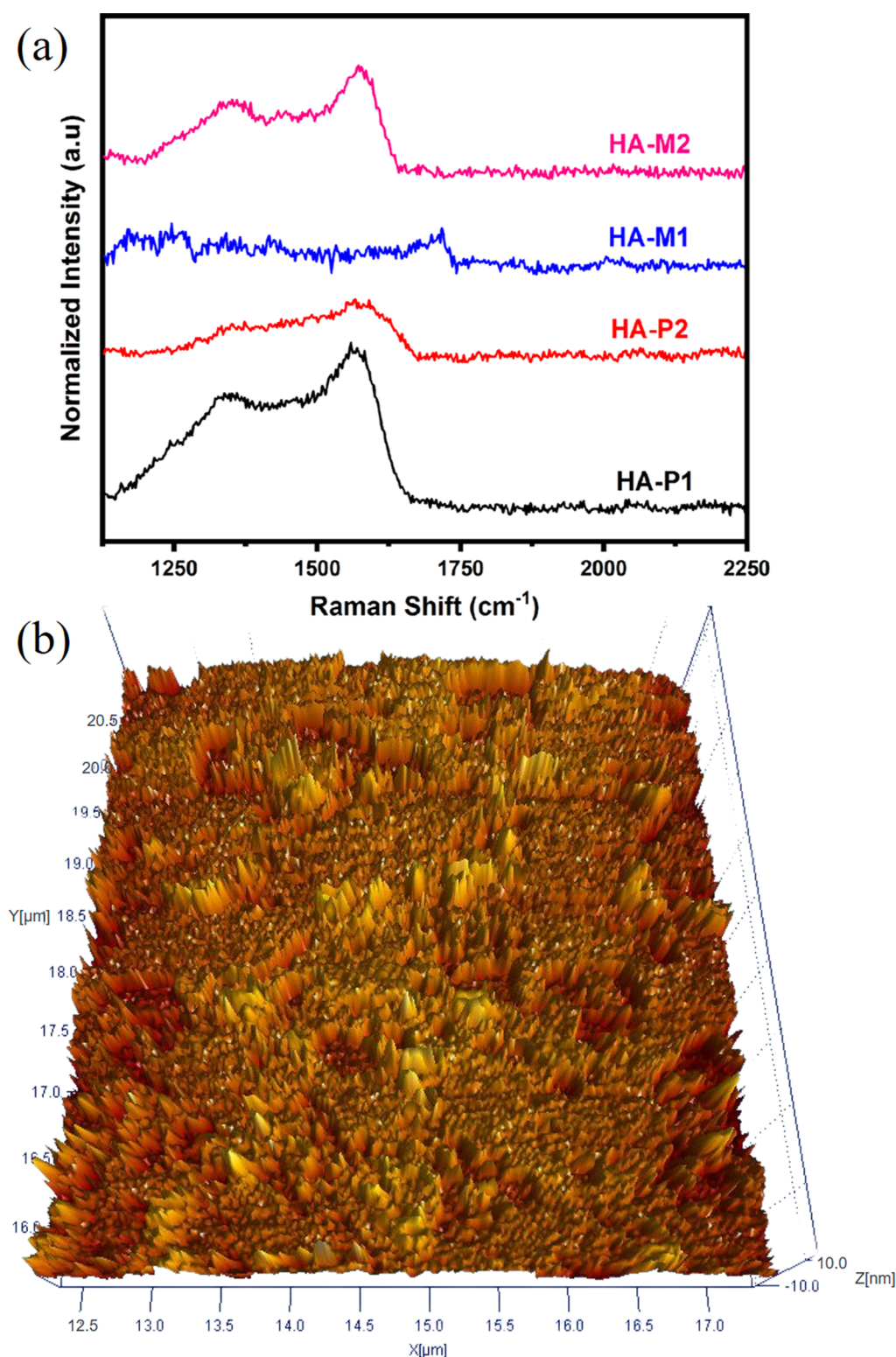
Figure 5. (a) Raman spectra of microwave-assisted CDs HA-M2 (purple line) and HA-M1 (blue line) and furnace-assisted CDs HA-P2 (red line) and HA-P1 (black line). (b) 3D topography of HA-P2.

incubating for 4 h. The reaction was stopped by adding a stopper reagent and then measuring the absorbance at 580 nm by an ELISA microplate reader.

4.4. Confocal Microscopic Imaging. The breast cancer cells (HeLa cells) were cultured by the CCK-8 assay (MedChemExpress, New Jersey, USA) in DMEM and incubated for 24 h. After that, they were incubated with CDs for 60 min. HeLa cells were washed three times with PBS to remove uninterpretable nanoparticles and fixed with 70% alcohol for 10 min at room temperature. A confocal laser scanning microscope, TCS SP2 (Leica Microsystems, USA), was used to take the cell images at an excitation wavelength of 488 nm.
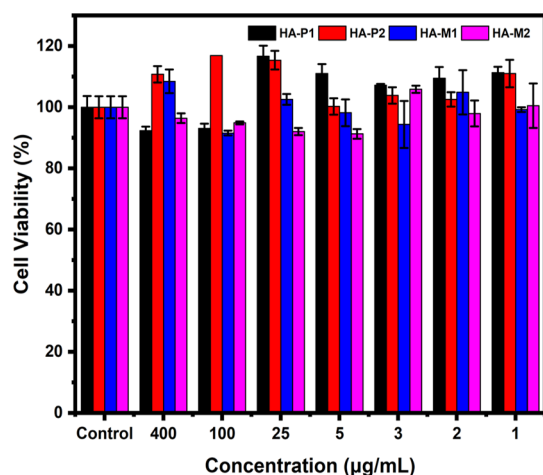
Figure 6. Varied concentrations of CDs HA-P1 (black bar), HA-P2 (red bar), HA-M1 (blue bar), and HA-M2 (purple bar). All data are represented as mean ± SD with $n = 3$.

4.5. Characterization. An X-ray diffractometer [Ultima IV Rigaku, USA, 18 kW with the rotating anode source Cu $K_{\alpha 1}$ line ($\lambda = 1.54$ Å)] was used to identify the crystal structure of CDs. Raman spectra [MRS-320 Raman Instrument system (Horiba Ltd, Japan)] identified the molecular interaction of CDs at an excitation wavelength of 532 nm. A Fourier transform infrared spectrophotometer [model IR Tracer-100 (Shimadzu, Japan)] was used to analyze the functional groups of CDs with the wavenumber ranging from 4000 to 400 cm^{-1} using the potassium bromide (KBr) pellet technique. A X-ray photoelectron spectrometer [Escalab 250Xi spectrometer with an Al $K\alpha$ radiation (hν = 1486.6 eV)] determined the composition of CDs. A spectrofluorometer (FluoroMax-4) and a UV−vis spectrophotometer (Shimadzu UV-1800) were used to measure fluorescence and absorbance spectra, respectively. The PL of the HA CDs was measured comparatively by

referring to rhodamine 6G [R6G, QY (95%)]; the % QY of HA CDs was determined by the following equation

$$QY = QY_{R6G}(I_{CDs}/I_{R6G})(A_{CDs}/A_{R6G})(\eta_{water}/\eta_{ethanol})^2$$

where I, A, and η are the integral PL intensity, UV absorbance and the optical density, and solvent reflective index, respectively.

4.6. Statistical Assessment. The CC_{50} of CDs was determined using the dose−response model (nonlinear fitting) of the Origin software (version 8.0724, OriginLab Inc., Northampton, MA). All data were obtained in triplicate, with the sample t-test performed on some data.

■ ASSOCIATED CONTENT

Ⓢ Supporting Information

The Supporting Information is available free of charge at https://pubs.acs.org/doi/10.1021/acsomega.1c01287.

> XRD diffractograms of HA-based CDs HA-M1, HA-M2, HA-P1, and HA-P2; AFM 2D morphology and size distribution of HA-P2; HeLa cancer cell viability curves after 24 h incubation for HA-M1, HA-M2, HA-P1, and HA-P2 using the microwave-assisted and furnace-assisted methods; CLSM images of HeLa cells using the z-stacking mode after 1 h treatment with HA-P2; and comparison of QY values of HA-based CDs (PDF)

■ AUTHOR INFORMATION

Corresponding Author

Mochamad Z. Fahmi − *Department of Chemistry and Supra Modification Nano-Micro Engineering Group, Universitas Airlangga, Surabaya 60115, Indonesia;* ⓞ orcid.org/0000-0001-5430-9992; Email: m.zakki.fahmi@fst.unair.ac.id
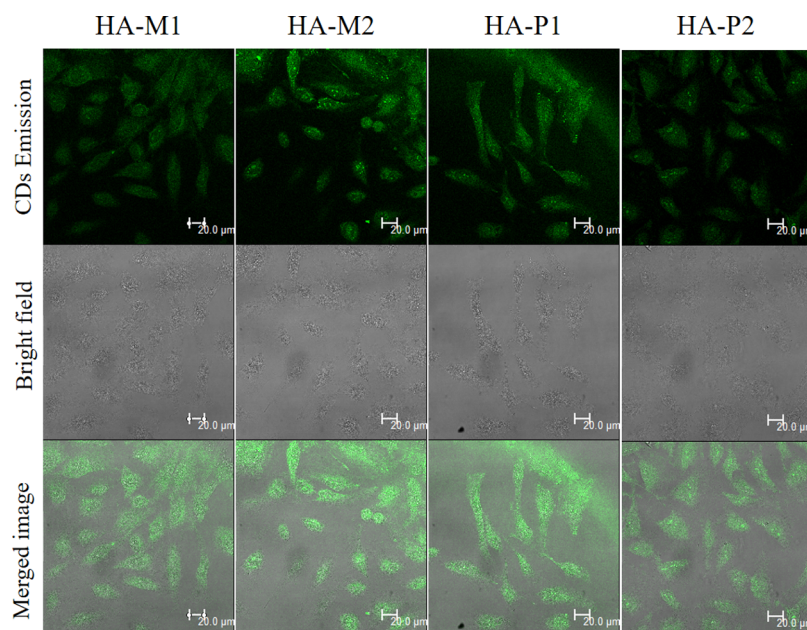
Figure 7. Photograph CLSM images of HeLa cells after 1 h incubation with HA-based CDs by excitation at 488 nm. The scale bars represent 20 μm.

Authors

Yu-Yu Aung − *Department of Chemistry, Universitas Airlangga, Surabaya 60115, Indonesia;* ● orcid.org/0000-0002-2169-4983

Aswandi Wibrianto − *Department of Chemistry, Universitas Airlangga, Surabaya 60115, Indonesia;* ● orcid.org/0000-0002-7746-7405

Jefry S. Sianturi − *Department of Chemistry, Universitas Airlangga, Surabaya 60115, Indonesia*

Desita K. Ulfa − *Department of Chemistry, Universitas Airlangga, Surabaya 60115, Indonesia*

Satya. C. W. Sakti − *Department of Chemistry and Supra Modification Nano-Micro Engineering Group, Universitas Airlangga, Surabaya 60115, Indonesia*

Irzaman Irzaman − *Department of Physics, IPB University, Bogor 16680, Indonesia*

Brian Yuliarto − *Department of Engineering Physics, Faculty of Industrial Technology, Institut Teknologi Bandung, Bandung 40116, Indonesia;* ● orcid.org/0000-0003-0662-7923

Jia-yaw Chang − *Department of Chemical Engineering, National Taiwan University of Science and Technology, Taipei, Taiwan 10607, Republic of China;* ● orcid.org/0000-0002-4172-6612

Yaung Kwee − *Department of Chemistry, Universitas Airlangga, Surabaya 60115, Indonesia*

Complete contact information is available at:
https://pubs.acs.org/10.1021/acsomega.1c01287

Notes

The authors declare no competing financial interest.

■ ABBREVIATIONS

CDs, carbon dots; QY, quantum yield; HA-P1, furnace-assisted carbon dots, 2 min; HA-P2, furnace-assisted carbon dots, 2 h; HA-M1, microwave-assisted carbon dots, 2 min; HA-M2, microwave-assisted carbon dots, 2 h; UV−vis, ultraviolet−visible light; PL, photoluminescence; FTIR, Fourier transform infrared; AFM, atomic force microscopy; CCK-8, cell counting kit 8; CLSM, confocal laser scanning microscopy; HA, hyaluronic acid; DMSO, dimethyl sulfoxide; NaOH, sodium hydroxide; C_2H_5OH, ethanol; DMEM, Dulbecco′s modified Eagle medium; PBS, phosphate-buffered saline; CC_{50}, 50% cytotoxic concentration; R6G, rhodamine 6G

■ REFERENCES

(1) Bray, F.; Ferlay, J.; Soerjomataram, I.; Siegel, R. L.; Torre, L. A.; Jemal, A. Global cancer statistics 2018: GLOBOCAN estimates of incidence and mortality worldwide for 36 cancers in 185 countries. *CA A Cancer J. Clin.* **2018**, *68*, 394−424.

(2) IARC. *Latest global cancer data: Cancer burden rises to 18.1 million new cases and 9.6 million cancer deaths in 2018*; International Agency for Research on Cancer: Lyon, France, 2018.

(3) Perumal, V.; Sivakumar, P. M.; Zarrabi, A.; Muthupandian, S.; Vijayaraghavalu, S.; Sahoo, K.; Das, A.; Das, S.; Payyappilly, S. S.; Das, S. Near infra-red polymeric nanoparticle based optical imaging in Cancer diagnosis. *J. Photochem. Photobiol., B* **2019**, *199*, 111630.

(4) Papadimitriou, S. A.; Salinas, Y.; Resmini, M. Smart polymeric nanoparticles as emerging tools for imaging—the parallel evolution of materials. *Chem.—Eur. J.* **2016**, *22*, 3612−3620.

(5) Fahmi, M. Z.; Chang, J.-Y. A facile strategy to enable nanoparticles for simultaneous phase transfer, folate receptor targeting, and cisplatin delivery. *RSC Adv.* **2014**, *4*, 56713−56721.

(6) Xu, X.; Lü, S.; Gao, C.; Wang, X.; Bai, X.; Gao, N.; Liu, M. Facile preparation of pH-sensitive and self-fluorescent mesoporous silica nanoparticles modified with PAMAM dendrimers for label-free imaging and drug delivery. *Chem. Eng. J.* **2015**, *266*, 171−178.

(7) Ghosh, D.; Bagley, A. F.; Na, Y. J.; Birrer, M. J.; Bhatia, S. N.; Belcher, A. M. Deep, noninvasive imaging and surgical guidance of submillimeter tumors using targeted M13-stabilized single-walled carbon nanotubes. *Proc. Natl. Acad. Sci. U.S.A.* **2014**, *111*, 13948−13953.

(8) Man, H. B.; Kim, H.; Kim, H.-J.; Robinson, E.; Liu, W. K.; Chow, E. K.-H.; Ho, D. Synthesis of nanodiamond−daunorubicin conjugates to overcome multidrug chemoresistance in leukemia. *Nanomed. Nanotechnol. Biol. Med.* **2014**, *10*, 359−369.

(9) Wegner, K. D.; Hildebrandt, N. Quantum dots: bright and versatile in vitro and in vivo fluorescence imaging biosensors. *Chem. Soc. Rev.* **2015**, *44*, 4792−4834.

(10) Saeed, A. A.; Sánchez, J. L. A.; O'Sullivan, C. K.; Abbas, M. N. DNA biosensors based on gold nanoparticles-modified graphene oxide for the detection of breast cancer biomarkers for early diagnosis. *Bioelectrochemistry* **2017**, *118*, 91−99.

(11) More, M. P.; Lohar, P. H.; Patil, A. G.; Patil, P. O.; Deshmukh, P. K. Controlled synthesis of blue luminescent graphene quantum dots from carbonized citric acid: Assessment of methodology, stability, and fluorescence in an aqueous environment. *Mater. Chem. Phys.* **2018**, *220*, 11−22.

(12) de Medeiros, T. V.; Manioudakis, J.; Noun, F.; Macairan, J.-R.; Victoria, F.; Naccache, R. Microwave-assisted synthesis of carbon dots and their applications. *J. Mater. Chem. C* **2019**, *7*, 7175−7195.

(13) Molaei, M. J. Carbon quantum dots and their biomedical and therapeutic applications: a review. *RSC Adv.* **2019**, *9*, 6460−6481.

(14) Wang, X.; Gao, T.; Yang, M.; Zhao, J.; Jiang, F.-L.; Liu, Y. Microwave-assisted synthesis, characterization, cell imaging of fluorescent carbon dots using l-asparagine as precursor. *New J. Chem.* **2019**, *43*, 3323−3331.

(15) Hill, S.; Galan, M. C. Fluorescent carbon dots from mono-and polysaccharides: synthesis, properties and applications. *Beilstein J. Org. Chem.* **2017**, *13*, 675−693.

(16) Shang, W.; Cai, T.; Zhang, Y.; Liu, D.; Liu, S. Facile one pot pyrolysis synthesis of carbon quantum dots and graphene oxide nanomaterials: all carbon hybrids as eco-environmental lubricants for low friction and remarkable wear-resistance. *Tribol. Int.* **2018**, *118*, 373−380.

(17) Choi, E. J.; Lee, J. M.; Youn, Y. S.; Na, K.; Lee, E. S. Hyaluronate dots for highly efficient photodynamic therapy. *Carbohydr. Polym.* **2018**, *181*, 10−18.

(18) Bukhari, S. N. A.; Roswandi, N. L.; Waqas, M.; Habib, H.; Hussain, F.; Khan, S.; Sohail, M.; Ramli, N. A.; Thu, H. E.; Hussain, Z. Hyaluronic acid, a promising skin rejuvenating biomedicine: A review of recent updates and pre-clinical and clinical investigations on cosmetic and nutricosmetic effects. *Int. J. Biol. Macromol.* **2018**, *120*, 1682−1695.

(19) Su, H.; Wang, J.; Yan, L. Homogeneously Synchronous Degradation of Chitin into Carbon Dots and Organic Acids in Aqueous Solution. *ACS Sustainable Chem. Eng.* **2019**, *7*, 18476−18482.

(20) Demir, B.; Lemberger, M. M.; Panagiotopoulou, M.; Medina Rangel, P. X.; Timur, S.; Hirsch, T.; Tse Sum Bui, B.; Wegener, J.; Haupt, K. Tracking hyaluronan: molecularly imprinted polymer coated carbon dots for cancer cell targeting and imaging. *ACS Appl. Mater. Interfaces* **2018**, *10*, 3305−3313.

(21) Tripodo, G.; Trapani, A.; Torre, M. L.; Giammona, G.; Trapani, G.; Mandracchia, D. Hyaluronic acid and its derivatives in

drug delivery and imaging: recent advances and challenges. *Eur. J. Pharm. Biopharm.* **2015**, *97*, 400−416.

(22) Wickens, J. M.; Alsaab, H. O.; Kesharwani, P.; Bhise, K.; Amin, M. C. I. M.; Tekade, R. K.; Gupta, U.; Iyer, A. K. Recent advances in hyaluronic acid-decorated nanocarriers for targeted cancer therapy. *Drug Discov. Today* **2017**, *22*, 665−680.

(23) Xu, X.; Ray, R.; Gu, Y.; Ploehn, H. J.; Gearheart, L.; Raker, K.; Scrivens, W. A. Electrophoretic analysis and purification of fluorescent single-walled carbon nanotube fragments. *J. Agron. Crop Sci.* **2004**, *126*, 12736−12737.

(24) Bottini, M.; Balasubramanian, C.; Dawson, M. I.; Bergamaschi, A.; Bellucci, S.; Mustelin, T. Isolation and characterization of fluorescent nanoparticles from pristine and oxidized electric arc-produced single-walled carbon nanotubes. *J. Phys. Chem. B* **2006**, *110*, 831−836.

(25) Sun, Y.-P.; Zhou, B.; Lin, Y.; Wang, W.; Fernando, K. A. S.; Pathak, P.; Meziani, M. J.; Harruff, B. A.; Wang, X.; Wang, H.; Luo, P. G.; Yang, H.; Kose, M. E.; Chen, B.; Veca, L. M.; Xie, S.-Y. Quantum-sized carbon dots for bright and colorful photoluminescence. *J. Agron. Crop Sci.* **2006**, *128*, 7756−7757.

(26) Zhao, Q.-L.; Zhang, Z.-L.; Huang, B.-H.; Peng, J.; Zhang, M.; Pang, D.-W. Facile preparation of low cytotoxicity fluorescent carbon nanocrystals by electrooxidation of graphite. *Chem. Commun.* **2008**, *41*, 5116−5118.

(27) Zheng, L.; Chi, Y.; Dong, Y.; Lin, J.; Wang, B. Electro-chemiluminescence of water-soluble carbon nanocrystals released electrochemically from graphite. *J. Agron. Crop Sci.* **2009**, *131*, 4564−4565.

(28) Wei, K.; Li, J.; Ge, Z.; You, Y.; Xu, H. Sonochemical synthesis of highly photoluminescent carbon nanodots. *RSC Adv.* **2014**, *4*, 52230−52234.

(29) Krysmann, M. J.; Kelarakis, A.; Dallas, P.; Giannelis, E. P. Formation mechanism of carbogenic nanoparticles with dual photoluminescence emission. *J. Agron. Crop Sci.* **2012**, *134*, 747−750.

(30) Sahu, S.; Behera, B.; Maiti, T. K.; Mohapatra, S. Simple one-step synthesis of highly luminescent carbon dots from orange juice: application as excellent bio-imaging agents. *Chem. Commun.* **2012**, *48*, 8835−8837.

(31) Gallo-Cordova, Á.; Espinosa, A.; Serrano, A.; Gutiérrez, L.; Menéndez, N.; del Puerto Morales, M.; Mazarío, E. New insights into the structural analysis of maghemite and (MFe 2 O 4, M= Co, Zn) ferrite nanoparticles synthesized by a microwave-assisted polyol process. *Mater. Chem. Front.* **2020**, *4*, 3063−3073.

(32) Li, J.; Li, M.; Tian, L.; Qiu, Y.; Yu, Q.; Wang, X.; Guo, R.; He, Q. Facile strategy by hyaluronic acid functional carbon dot-doxorubicin nanoparticles for CD44 targeted drug delivery and enhanced breast cancer therapy. *Int. J. Pharm.* **2020**, *578*, 119122.

(33) Wang, H.-J.; Zhang, J.; Liu, Y.-H.; Luo, T.-Y.; He, X.; Yu, X.-Q. Hyaluronic acid-based carbon dots for efficient gene delivery and cell imaging. *RSC Adv.* **2017**, *7*, 15613−15624.

(34) Zhang, L.; Lin, Z.; Yu, Y.-X.; Jiang, B.-P.; Shen, X.-C. Multifunctional hyaluronic acid-derived carbon dots for self-targeted imaging-guided photodynamic therapy. *J. Mater. Chem. B* **2018**, *6*, 6534−6543.

(35) Qu, D.; Zheng, M.; Zhang, L.; Zhao, H.; Xie, Z.; Jing, X.; Haddad, R. E.; Fan, H.; Sun, Z. Formation mechanism and optimization of highly luminescent N-doped graphene quantum dots. *Sci. Rep.* **2014**, *4*, 1−11.

(36) Wibrianto, A.; Khairunisa, S. Q.; Sakti, S. C. W.; Ni'mah, Y. L.; Purwanto, B.; Fahmi, M. Z. Comparison of the effects of synthesis methods of B, N, S, and P-doped carbon dots with high photoluminescence properties on HeLa tumor cells. *RSC Adv.* **2021**, *11*, 1098−1108.

(37) Wang, B.-B.; Jin, J.-C.; Xu, Z.-Q.; Jiang, Z.-W.; Li, X.; Jiang, F.-L.; Liu, Y. Single-step synthesis of highly photoluminescent carbon dots for rapid detection of Hg2+ with excellent sensitivity. *J. Colloid Interface Sci.* **2019**, *551*, 101−110.

(38) Wu, Z. L.; Liu, Z. X.; Yuan, Y. H. Carbon dots: materials, synthesis, properties and approaches to long-wavelength and multi-color emission. *J. Mater. Chem. B* **2017**, *5*, 3794−3809.

(39) Bhartiya, P.; Singh, A.; Kumar, H.; Jain, T.; Singh, B. K.; Dutta, P. Carbon dots: Chemistry, properties and applications. *J. Indian Chem. Soc.* **2016**, *93*, 759−766.

(40) Lawson-wood, K.; Upstone, S.; Evans, K., Determination of Relative Fluorescence Quantum Yields using the FL6500 Fluorescence Spectrometer. *Fluorescene Spectroscopy*; PerkinElmer Inc.: Seer Green, U.K., 2018.

(41) Fang, Q.; Dong, Y.; Chen, Y.; Lu, C.-H.; Chi, Y.; Yang, H.-H.; Yu, T. Luminescence origin of carbon based dots obtained from citric acid and amino group-containing molecules. *Carbon* **2017**, *118*, 319−326.

(42) Pudza, M. Y.; Abidin, Z. Z.; Abdul-Rashid, S.; Yassin, F. M.; Noor, A. S. M.; Abdullah, M. Synthesis and Characterization of Fluorescent Carbon Dots from Tapioca. *ChemistrySelect* **2019**, *4*, 4140−4146.

(43) Huang, J. J.; Zhong, Z. F.; Rong, M. Z.; Zhou, X.; Chen, X. D.; Zhang, M. Q. An easy approach of preparing strongly luminescent carbon dots and their polymer based composites for enhancing solar cell efficiency. *Carbon* **2014**, *70*, 190−198.

(44) Thakur, M.; Mewada, A.; Pandey, S.; Bhori, M.; Singh, K.; Sharon, M.; Sharon, M. Milk-derived multi-fluorescent graphene quantum dot-based cancer theranostic system. *Mater. Sci. Eng. C* **2016**, *67*, 468−477.

(45) Xu, D.; Lei, F.; Chen, H.; Yin, L.; Shi, Y.; Xie, J. One-step hydrothermal synthesis and optical properties of self-quenching-resistant carbon dots towards fluorescent ink and as nanosensors for Fe 3+ detection. *RSC Adv.* **2019**, *9*, 8290−8299.

(46) Fahmi, M. Z.; Haris, A.; Permana, A. J.; Nor Wibowo, D. L.; Purwanto, B.; Nikmah, Y. L.; Idris, A. Bamboo leaf-based carbon dots for efficient tumor imaging and therapy. *RSC Adv.* **2018**, *8*, 38376−38383.

(47) Prasannan, A.; Imae, T. One-pot synthesis of fluorescent carbon dots from orange waste peels. *Ind. Eng. Chem. Res.* **2013**, *52*, 15673−15678.

(48) Aung, Y. Y.; Kristanti, A. N.; Khairunisa, S. Q.; Nasronudin, N.; Fahmi, M. Z. Inactivation of HIV-1 Infection through Integrative Blocking with Amino Phenylboronic Acid Attributed Carbon Dots. *ACS Biomater. Sci. Eng.* **2020**, *6*, 4490−4501.

(49) Mathew, S. A.; Praveena, P.; Dhanavel, S.; Manikandan, R.; Senthilkumar, S.; Stephen, A. Luminescent chitosan/carbon dots as an effective nano-drug carrier for neurodegenerative diseases. *RSC Adv.* **2020**, *10*, 24386−24396.

(50) Stepanidenko, E. A.; Arefina, I. A.; Khavlyuk, P. D.; Dubavik, A.; Bogdanov, K. V.; Bondarenko, D. P.; Cherevkov, S. A.; Kundelev, E. V.; Fedorov, A. V.; Baranov, A. V.; Maslov, V. G.; Ushakova, E. V.; Rogach, A. L. Influence of the solvent environment on luminescent centers within carbon dots. *Nanoscale* **2020**, *12*, 602−609.

(51) Zafar, Z.; Ni, Z. H.; Wu, X.; Shi, Z. X.; Nan, H. Y.; Bai, J.; Sun, L. T. Evolution of Raman spectra in nitrogen doped graphene. *Carbon* **2013**, *61*, 57−62.

(52) Kütahya, C.; Wang, P.; Li, S.; Liu, S.; Li, J.; Chen, Z.; Strehmel, B. Carbon dots as a promising green photocatalyst for free radical and ATRP-based radical photopolymerization with blue LEDs. *Angew. Chem., Int. Ed.* **2020**, *59*, 3166−3171.

(53) Zhang, Z.; Yi, G.; Li, P.; Zhang, X.; Fan, H.; Zhang, Y.; Wang, X.; Zhang, C. A minireview on doped carbon dots for photocatalytic and electrocatalytic applications. *Nanoscale* **2020**, *12*, 13899−13906.

(54) Wang, H.; Cao, J.; Zhou, Y.; Wang, Z.; Zhao, Y.; Liu, Y.; Huang, H.; Shao, M.; Liu, Y.; Kang, Z. Carbon dot-modified mesoporous carbon as a supercapacitor with enhanced light-assisted capacitance. *Nanoscale* **2020**, *12*, 17925−17930.

(55) Ansari, M. A.; Pedergnana, V.; Pedergnana, V.; L C Ip, C.; Magri, A.; Von Delft, A.; Bonsall, D.; Chaturvedi, N.; Bartha, I.; Smith, D.; Nicholson, G.; McVean, G.; Trebes, A.; Piazza, P.; Fellay, J.; Cooke, G.; Foster, G. R.; Hudson, E.; McLauchlan, J.; Simmonds, P.; Bowden, R.; Klenerman, P.; Barnes, E.; Spencer, C. C. A. Genome-

to-genome analysis highlights the effect of the human innate and adaptive immune systems on the hepatitis C virus. *Nat. Genet.* **2017**, *49*, 666.

(56) Capáková, Z.; Radaszkiewicz, K. A.; Acharya, U.; Truong, T. H.; Pacherník, J.; Bober, P.; Kašpárková, V.; Stejskal, J.; Pfleger, J.; Lehocký, M.; Humpolíček, P. The biocompatibility of polyaniline and polypyrrole 2: Doping with organic phosphonates. *Mater. Sci. Eng. C* **2020**, *113*, 110986.

(57) Kanagasubbulakshmi, S.; Lakshmi, K.; Kadirvelu, K. Carbon quantum dots-embedded electrospun antimicrobial and fluorescent scaffold for reepithelialization in albino wistar rats. *J. Biomed. Mater. Res.* **2020**, *109*, 637.

(58) Shen, J.; Zhu, Y.; Yang, X.; Li, C. Graphene quantum dots: emergent nanolights for bioimaging, sensors, catalysis and photovoltaic devices. *Chem. Commun.* **2012**, *48*, 3686−3699.

(59) Wang, Z.; Tian, Y.; Zhang, H.; Qin, Y.; Li, D.; Gan, L.; Wu, F. Using hyaluronic acid-functionalized pH stimuli-responsive mesoporous silica nanoparticles for targeted delivery to CD44-overexpressing cancer cells. *Int. J. Nanomed.* **2016**, *11*, 6485.

(60) Yu, M.; Jambhrunkar, S.; Thorn, P.; Chen, J.; Gu, W.; Yu, C. Hyaluronic acid modified mesoporous silica nanoparticles for targeted drug delivery to CD44-overexpressing cancer cells. *Nanoscale* **2013**, *5*, 178−183.